Force-State Mapping Identification of Nonlinear Joints

Edward F. Crawley* and Kevin J. O'Donnell†
Massachusetts Institute of Technology, Cambridge, Massachusetts

A procedure is presented for identifying the potentially strong nonlinear properties of structural members, such as joints, by expressing the force transmitted by the member as a function of its mechanical state. By explicitly including position- and rate-dependent effects, the surface of the transmitted force vs state—the force-state map—has distinct, unique, superposable features for common structural nonlinearities, even those that appear to indicate hysteresis on a force-stroke presentation. An analysis is performed on the influence of true memory effects, transient response, and uncertainty in the measurements and system mass on the precision of the procedure. The successful identification of simulated data verifies the accuracy of the identification algorithm. Tests are then conducted on three actual joint models, with incomplete state measurements typical of an actual testing environment. The ability of the procedure to estimate the complete state vector and to analyze and reconstruct the measured nonlinear characteristics is demonstrated.

Nomenclature

A = state space dynamics matrix
B = control effectiveness matrix
b,B = linear viscous damping value
B_{DB} = deadband viscous damping value
C = observability matrix
f = memory dynamics function
F = force applied to joint
F_F = friction force value
F_T = transmitted force
g = displacement-dependent friction damping
k,K = linear stiffness value
K_{DB} = deadband stiffness value
K_3 = cubic spring stiffness value
K = feedback gain matrix
M = mass
p = inverse memory time constant
u = control matrix
$\hat{v}$ = estimated velocity
v = disturbance noise matrix
w = measurement noise matrix
x = state matrix
$\hat{x}$ = state estimate
y = measurement matrix
ϵ = error matrix
η = measurement noise
κ = convolution memory constant
ω_0 = undamped natural frequency

Introduction

WITH the current use of the Space Shuttle as the primary mode of transportation to orbit, the design of space structures must be based on the use of compact components that are either deployed or assembled on orbit. When considering the design and analysis of such structures, the connecting elements (the joints) play an important part in the overall dynamics of the system. The linear stiffness characteristics of the joints will influence the frequencies and mode shapes of the final structure. In addition, the joints are seen as a potentially major source of damping and nonlinear behavior. An understanding of how the nonlinear system parameters change with amplitude and frequency is especially important when designing an active control system for such a structure.

Current techniques of investigating the dynamics of structures include modal and transient identification techniques.[1-3] These methods are based on the assumption of linearity of the system and have been shown to work to a limited extent in the presence of weak nonlinearities. In the presence of locally strong nonlinearities such as joints, simple load stroke or force-displacement testing has been used.[4] Such force-displacement testing yields only a partial state space representation of the joint characteristics; i.e., the force transmitted by the joint is determined as a function of its displacement. Force effects that depend on the velocity or on the true memory effect in the joint are not explicitly displayed and can only be incompletely inferred from the hysteritic behavior shown on the force-displacement diagram.

As an alternative to these techniques, a new technique know as force-state mapping has been developed.[5,6] In the force-state mapping technique, the force transmitted by the joint is represented as function of the displacement and velocity across the joint, i.e., as a function of the full mechanical state of the joint. In contrast to the force-displacement method, this technique provides sufficient information to identify the rate-dependent effects associated with the joint. In addition, the explicit presentation of the velocity dependence allows differentiation of hysteritic behavior as either time-invariant rate effects of time-dependent memory effects. Finally, the presentation of the data as a force surface in the state space of displacement and velocity makes it readily available for direct incorporation into time marching numerical calculations of the response of a nonlinear structure of which the joint is an element.

This paper addresses the subject of identifying the strong nonlinearities in actual space joints such as friction, impacts, and deadbands by using the force-state mapping technique. First, a formal presentation of the force-state mapping technique will be presented, along with a discussion of the effects of memory in the system and their incorporation into the technique. Critical aspects of the experimental approach will then be discussed, including an estimation technique for determining full state estimates from partial state measurements, the sensor selection, and the experimental setup. In

Received March 21, 1986; presented as Paper 86-1013 at the AIAA/ASME/ASCE/AHS 27th Structures, Structural Dynamics and Materials Conference, San Antonio, TX, May 19-21, 1986; revision received Oct. 3, 1986.

*Associate Professor, Department of Aeronautics and Astronautics. Member AIAA.
†Research Assistant. Department of Aeronautics and Astronautics. Member AIAA.

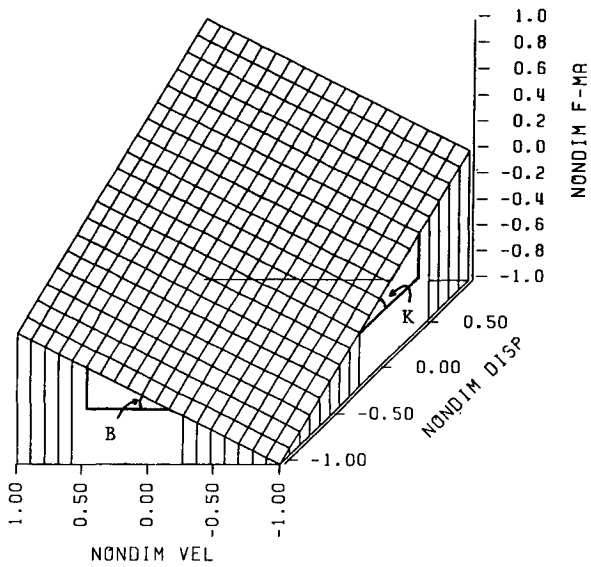

Fig. 1 Force-state map of an ideal linear spring damper.

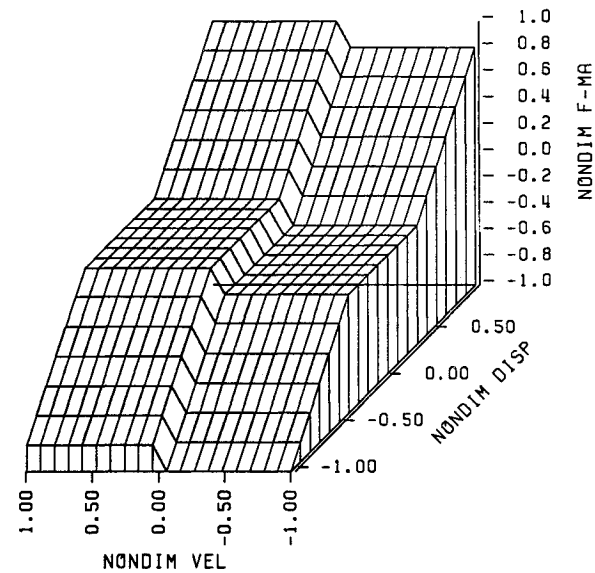

Fig. 2 Force-state map of an ideal deadband spring with Coulomb friction.

order to validate the estimation and identification procedure, nonlinear analog computer simulations were used to produce data of known system content. These data were then identified with the force-state approach and the original and identified parameters were compared. Finally, several actual joint models were experimentally tested and identified. The ability to identify and decompose the behavior of a complicated joint model into basic nonlinearities will be demonstrated and verified.

Analytic Foundation of Force-State Mapping

In this section, the force-state mapping technique will be formally described for a single-degree-of-freedom nonlinear spring mass damper system. One example of this type of system might be the axial load transfer through a space truss joint, where the spring and damper are properties of the joint, and the mass of the system is the mass of the adjacent truss element. In comparison to the relatively slow dynamics of the entire structure, a single-degree-of-freedom model is expected to accurately represent in a quasisteady sense the relatively fast local dynamics associated with the joint. The state of the joint is completely described by the local displacement x and velocity $\dot{x}$ across the joint. The dynamics associated with this model can be represented by the memoryless ordinary nonlinear second-order equation of motion

$$M\ddot{x}+B(x,\dot{x})\dot{x}+K(x,\dot{x})x=F(t) \tag{1}$$

where the generalized damping and stiffness B and K can vary as a function of the state. Equation (1) is sufficiently general to describe any constant-mass, memoryless, single-degree-of-freedom system. The effect of memory on the system will be addressed below. Regrouping the terms of Eq. (1) gives

$$F_\tau(x,\dot{x})=B(x,\dot{x})\dot{x}+K(x,\dot{x})x=F(t)-M\ddot{x} \tag{2}$$

where F_τ represents the force transmitted by the joint entirely as a function of the instantaneous state of the joint.

The objective of the force-state mapping approach is to produce a plot of the transmitted force F_τ as a function of the state. This plot would be a three-dimensional surface of F_τ vs x and $\dot{x}$ for a memoryless single-degree-of-freedom model and is referred to as a force-state map. To generate the force-state map of a joint, measurements of the displacement, velocity, acceleration and applied force are required at each time interval. The force-state map of a general linear spring mass damper system produces an inclined plane whose slope with respect to displacement is the linear stiffness K and with respect to velocity is the linear viscous damping B (Fig. 1).

Any evidence that a force-state map is other than a plane is an indication of a nonlinearity in the system. Different types of nonlinearities will, in general, produce distinct force-state maps. An important characteristic of the force-state mapping technique is its ability to display superposable nonlinearities. This property is based on the ability to express the transmitted force [Eq. (2)] as the linear combination of linear and nonlinear force components. Experience has shown that a relatively small set of describing force components can provide an accurate reconstruction of the trasmitted force. A representative, but not exhaustive, list of such force components is given as

$$F_\tau=C+K_1x+B_1\dot{x}+K_nx^n+B_n\dot{x}^n+K_{DB}+B_{DB}+F_F\,\mathrm{sign}(\dot{x})+g\,|x|\,\mathrm{sign}(\dot{x}) \tag{3}$$

with

$$K_{DB}=\begin{cases}k_{DB}(x-x_{DB}) & \\ 0 & , \\ k_{DB}(x+x_{DB}) & \end{cases} \qquad B_{DB}=\begin{cases}b_{DB}(\dot{x}) & x_{DB}\le x \\ 0 & -x_{DB}\le x\le x_{DB} \\ b_{DB}(\dot{x}) & x\le -x_{DB}\end{cases}$$

where the first three terms of Eq. (3) represent a constant preload, a linear spring, and a linear damper. The next two terms represent higher-order springs and dampers, the sixth and seventh terms deadband springs and dampers, the eighth classical Coulomb friction, and the last classical $(1+ig)$ material hysteresis damping and displacement dependent friction.[7]

The intent of describing the transmitted force by common nonlinearities is not to rigorously identify all of the internal phenomena causing the measured response, but rather to approximately model the joint as it is seen by the structure around the joint. Included in Eq. (3) are most of the contributions to so-called "hysteresis" or "memory" effects on a conventional load-stroke plot. It should be emphasized that these are not true memory effects, but depend only on the instantaneous state. Therefore, each will produce a

distinct, unique, superposable surface on a force-state map, independent of the amplitude, frequency, or time history of the test. As an example, the force-state map of a typical nonlinear joint might include a deadband due to play in the joint and classical Coulomb friction between moving surfaces as depicted in Fig. 2. With the property of superposition, a designer can easily visualize what nonlinear effects, if any, are present in a given joint or structure and then analyze their significance on the dynamics of the system.

There are, however, instances when the transmitted force does depend on the specific time history of the motion. True memory effects include viscoelastic responses such as creep and force transmitted during load cycles in which material plasticity is encountered. To evaluate the effect of a memory component on the transmitted force, memory dynamics are now included in the expression for the transmitted force,

$$F_T = K(x,\dot{x})x + B(x,\dot{x})\dot{x} + \kappa\int Q(x,\dot{x})\,dt \tag{4}$$

where the additional term represents the memory of the system as an integral in time over some possibly nonlinear function of the state time history. For the special case of a memory effect that is linearly related to the state, the last term in Eq. (4) can be rewritten in the form of a convolution integral of the state. This can equivalently be represented by the addition of an augmented state variable describing the memory dynamics, as

$$F_T = K(x,\dot{x})x + B(x,\dot{x})\dot{x} + \kappa q(t)$$
$$\dot{q} = f(q,x,\dot{x}) \tag{5}$$

It is desirable to see how an example of a linear memory effect will influence the force-state map. Assuming a system composed of a linear spring, no damper, and the memory effect in Eq. (5) as a simple first-order lag on the velocity,

$$\dot{q} + pq = \dot{x} \tag{6}$$

the transmitted force of the spring mass memory system can be calculated at a fixed frequency. Such a force-state map will appear as an inclined plane with apparent effective linear stiffness and damping similar to Fig. 1. Thus, linear instantaneous rate-dependent damping and linear memory effects can give the appearance of the same force-state map. This implies that, without prior knowledge, a single test cannot differentiate between a spring-damper combination and the presence of a linear-related memory component. However, the planar inclinations of the memory induced force-state map change with frequency,[5] whereas the system with no memory will retain the same stiffness and damping slopes regardless of frequency. Therefore, a simple way to distinguish between true memory and simple rate-dependent effects is by performing several tests with different input frequencies.

Once the presence of memory has been confirmed, the force-state mapping technique can be modified to accurately represent the system dynamics. If the paramaters describing the dynamics of the memory equation [Eq. (5)] can be identified, or accurately approximated from the force-state map or from external analysis, a new higher-dimensional force-state map independent of frequency can still be created with the effects of memory treated as an augmented state variable. If the presence of true memory effects is confirmed, but cannot be isolated as an augmented state, the alternative is to test the joint only at the frequencies of interest.

The analytic foundation of force-state mapping can be summarized as follows. For the majority of systems, the force-state map will be unique, independent of frequency, and composed of superposable linear and nonlinear effects. This class of systems will include the vast majority of dynamic systems that operate sufficiently fast that creep is not important and at low enough amplitudes that plasticity is not encountered. For such systems with true memory effects, augmented memory states must be identified or testing done at appropriate frequencies and amplitudes.

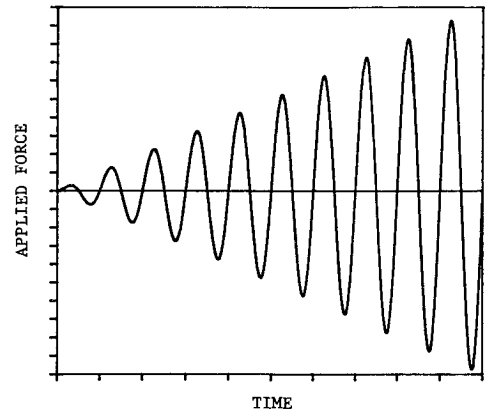

Fig. 3 Time history of the applied excitation force.

Implementation of Force-State Mapping

Implementation of the force-state mapping technique requires 1) selection and application of the excitation force $F(t)$ applied to the system, 2) processing the system response to construct the force-state map, and 3) extraction of the pertinent system parameters from the map. The issues of the applied force and data processing are discussed below. Extraction of system parameters will be discussed in the context of analyzing the analog simulation data.

State Measurement and Estimation

In the previous section, it was stated that in order to construct the force-state map, the displacement, velocity, acceleration, and applied force must be obtained as a function of time. To obtain these synchronized signals independently, four separate sensors are needed, each with identical time delay characteristics. Rather than measure each signal independently, a software estimation filter can be used to obtain estimates of $x,\dot{x},\ddot{x}$ from partial state measurements. This technique allows for fewer experimental measurements and incorporates all of the information contained in each of these measurements into the estimates of all of the states. An approach to consistently estimating states from a limited number of measurements is found in estimation theory. In this somewhat unusual application of estimation theory, the dynamics to be modeled are those relating to measurements (i.e., a double integrator from acceleration to displacement) with the noisy acceleration measurement as the "driving input" and the "measurements" as the measured noisy states.[8,9] For the case in which only the acceleration and displacement are measured, the equations for the measurement dynamics can be written as

$$\begin{bmatrix}\dot{x}\\ \ddot{x}\end{bmatrix} = \begin{bmatrix}0 & 1\\ 0 & 0\end{bmatrix}\begin{bmatrix}x\\ \dot{x}\end{bmatrix} + \begin{bmatrix}0\\ 1\end{bmatrix}\ddot{x}_m + \begin{bmatrix}0\\ 1\end{bmatrix}\eta_a \tag{7}$$

$$y = x_m = [1 \quad 0]\begin{bmatrix}x\\ \dot{x}\end{bmatrix} + \eta_d \tag{8}$$

where the bias and noise errors in each measurement have been removed and placed in the η terms. Equations (7) and (8) can be rewritten in matrix form as

$$\dot{x} = Ax + Bu + v \tag{9}$$

$$y = Cx + w \tag{10}$$

where v and w describe the noise in the accelerometer and displacement transducer, respectively. Equations (9) and (10) are identities that do not depend on the choice of the estimation filter or the potentially nonlinear dynamics of the structure. They rigorously represent the linear relationships between the states, the measurements, and the associated noises. In this formulation, the equations are of a form in which modern state estimation techniques can be applied. The standard feedback estimation formulation for the state estimates $\hat{x}$ is of the form

$$\dot{\hat{x}} = A\hat{x} + Bu + K(y - C\hat{x}) \tag{11}$$

where $K = [k_1 \ k_2]^T$ represents the desired feedback gains of the estimator. The final design of the estimator included an augmented error state to eliminate errors due to integrations of a steady-state accelerometer bias error (see Appendix).

Once the method of obtaining the force and state measurements is determined, the remaining piece of information necessary for the determination of the transmitted force is the overall effective system mass. Methods of calculating the system mass include direct measurement, analytic calculation, or an independent parameter identification technique. The method used will strongly depend on the type of structure being tested.

Once the measurements are obtained and the mass is known, a force-state map can be created by computing the transmitted force at each time point that is equal to the applied force minus the inertial force. The state space is then partitioned into a grid and the transmitted force at each grid element is calculated as the average of the transmitted forces from all measurements within the element.

Excitation Force Specification

The fundamental force-state formulation [Eq. (2)] indicates that the sensitivity of the measured transmitted force to the mass is proportional to the relative magnitude of the inertial force compared to the applied force. Below the first natural frequency, the inertial force is relatively small compared to the applied force and, therefore, the transmitted force is relatively insensitive to the uncertainty in the mass. Above the natural frequency, the inertial force becomes significant compared to the applied force and algebraically subtracts from it. Therefore, the transmitted force characteristics should be measured at forcing frequencies well below the first natural frequency of the structure being tested in order to minimize the effects of uncertainty in the system mass.

The ability to produce complete force-state maps also requires that the force input waveform excite displacements and velocities that adequately span the state space in such a way that the measurements are reasonably dense within the space. If the measurements are not dense, a region in the state space is created near which no transmitted force information has been measured, producing a "hole" in the surface of the force-state map. A modulated sinusoid, which monotonically increases in amplitude from zero to some final value, will produce an increasing spiral shape in the state space and, within the limits of the maximum displacement and velocity, provide a fairly dense set of measurement points (Fig. 3). The actual waveform used is also modulated back to zero amplitude so that the state space is spanned twice.

Table 1 Identified parameters of the cubic spring simulation data

K_{rel}	K_{meas}/K_{act}	B_{meas}/B_{act}	K_{3meas}/K_{3act}
1.00	1.00067	1.00906	0.98529
1.25	1.00017	0.99438	0.99174
0.87	1.00052	1.00292	0.98135
0.00	1.00026	1.01867	—
5.32	0.99867	0.96284	0.99617
1.08	1.00040	1.01832	0.98651
1.02	1.00060	1.00467	0.98348
0.62	1.00039	1.00525	0.98192
Average	1.00021	1.00201	0.98664
RMS error, %	±0.060	±1.66	±0.512

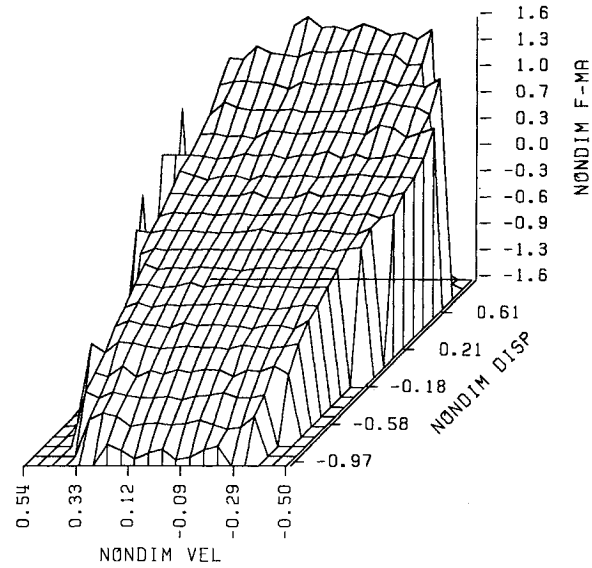

Fig. 4 Force-state map of a simulated spring mass damper system with a cubic spring.

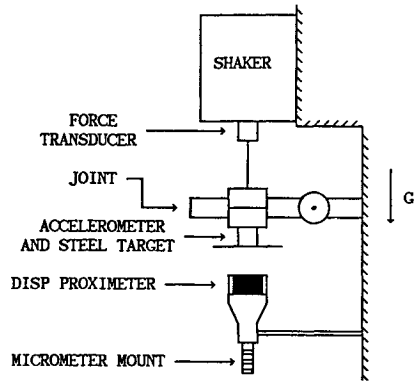

Fig. 5 Experimental configuration.

Since the applied force input is not a steady-state excitation, it will produce both homogeneous and nonhomogeneous response from the joint. The transient response of the joint can be obtained from Eq. (1) with the applied force $F(t)$ set to zero. From Eq. (2), the transmitted force due to the transient is identical to that due to the forced response. The force-state map will not be affected by the presence of transient responses in the total response, since they will overplot onto the same force-state characteristics. The dynamics associated with the shaker are eliminated by measuring the applied force with a force transducer attached to the structure at the point of force application. Thus,

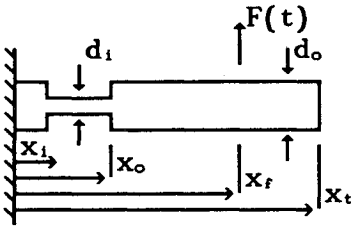

Fig. 6 Notched rod test specimen.

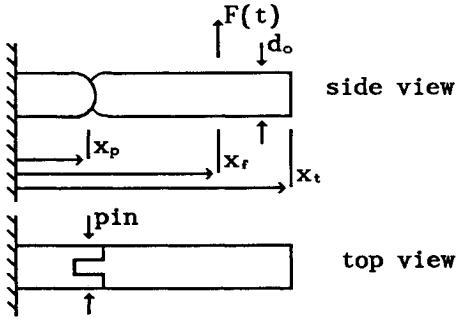

Fig. 7 Pinned clevis joint test specimen.

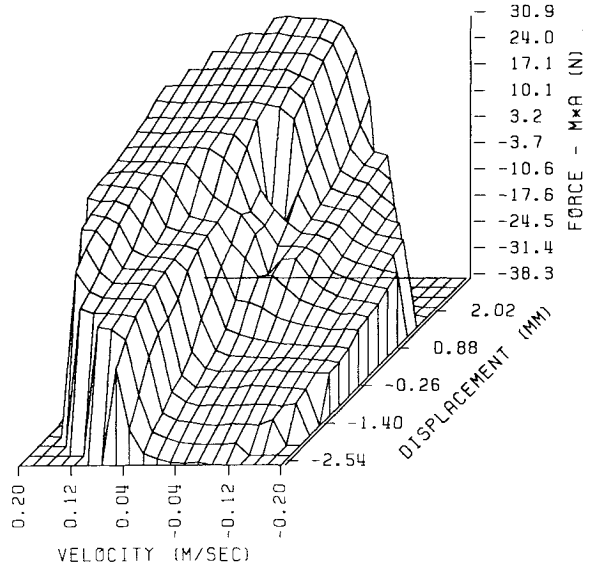

Fig. 8 Experimentally measured force-state map of a pinned clevis joint.

Table 2 Sensor specifications

Sensor	Range	BW, Hz	Linearity, %
Displacement proximeter	±5 mm	0–10000	±1
Accelerometer	±25 g	0–2000	±1
Force transducer	±100 lbf	0.005-6000	±1

Table 3 Notched rod properties

x_i = 38.25 mm	d_i = 15.88 mm
x_0 = 88.25 mm	d_0 = 31.75 mm
x_f = 246.89 mm	E = 73.03 GPa
x_t = 340.61 mm	

neither the transient dynamics of the system nor the shaker adversely affect the construction of the force-state map.

Computer Simulations

Having laid the foundation of the force-state mapping technique, the next task is the application of the technique to the identification of nonlinear dynamic systems. Typically, the process of identification becomes complicated when noise is present in the measurements or when the type of nonlinearity affecting the system is not well understood. In this section, the force-state mapping technique is applied to the simple case in which the type of nonlinearities are known in advance and the signals are free of measurement noise.

To provide the data on the response of a nonlinear system, a cubic spring nonlinearity was added to a spring mass damper system and the equation of motion was programmed on an EAI 8000 analog computer. The input to the system was identical to that to be used in the experiment, as described in the previous section. The modulated input frequency was programmed at one-sixth of the damped natural frequency of the spring mass damper system in Eq. (12). The resulting signals of force, acceleration, velocity, and displacement were then recorded at 100 times the input frequency to assure accurate sampling of the state space. The system was not programmed with any memory effects and the measurements are accurate to the resolution of the analog computer, one part is 40,000 for full-scale signals.

As described, a cubic spring analog simulation was tested as defined by

$$M\ddot{x}+B\dot{x}+Kx+K_3x^3=F(t) \tag{12}$$

To obtain the system parameters that best describe the transmitted force, a three-dimensional surface was fit to the force-state maps of the model using a least squares algorithm with the displacement and velocity as independent variables. The equation of motion given in Eq. (12) was used as the functional form of the surface. In this manner, only the terms of Eq. (3) known to be present in the system were used in the surface fit. A comparison between the measured and programmed values of the linear spring, linear damper, and cubic spring parameters is shown in Table 1, where K_{rel} is simply a measure of the relative amount of cubic stiffness compared to a base level.

The data in Table 1 indicate excellent agreement of the measured system parameters with their programmed values. This is an important controlled test in that it demonstrates that the force-state mapping technique is capable of representing and identifying the complete system parameters when the exact nature of the nonlinearity is known and when no noise is present in the system.

A force-state map representative of the cubic spring nonlinearity is shown in Fig. 4. The cubic dependence on displacement is apparent, but the linear viscous damping dependence is not clear. This is due to the fact that the damping present corresponds to less the 1% critical damping, which is common in most structures, but difficult to notice on the force-state map. However, the combination of the linear and cubic springs demonstrate that this figure is a good example of the ability to superpose the linear and nonlinear effects in the force-state space.

This simulation study also discovered an important fact about fitting nonlinear functions to the force-state map. The cubic spring nonlinearity discussed above and most types of friction nonlinearities are similar in that the functional form of the nonlinearity does not change with the state variables. However, Eq. (3) shows that the actual form of the deadband nonlinearity changes with displacement. Therefore, common least squares algorithms cannot be used to fit to force-state surfaces with deadbands.

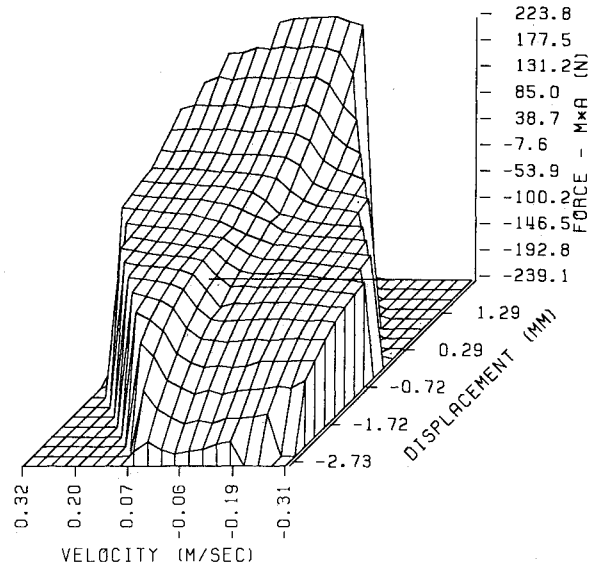

Fig. 9 Experimentally measured force-state map of a pinned clevis joint with sleeve.

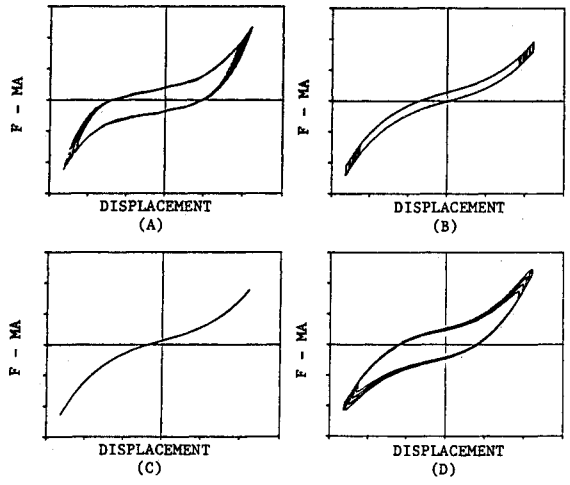

Fig. 10 Reconstruction of the force-state map of Fig. 9 using the identified fit parameters.

Experimental Description

Test Setup

In the section on implementation, estimation techniques were proposed for measuring the system mass and also for estimating the full state of the joint from measurements of the displacement, acceleration, and applied force, measurements commonly made in a dynamics laboratory. This section will describe the actual experimental setup used and the various joint specimens tested.

The selection of specific sensors will, of course, depend on the expected maximum frequency and amplitude of the envisioned test. For the experiments performed, a Ling model 420-1B electromagnetic shaker (maximum force 100 lb) was used to apply the external excitation forcing, which was measured by the PCB model 208A02 piezoelectric force transducer. Since emphasis was given to low-frequency tests, the Endevco model 2262-25 piezoresistive accelerometer was chosen. Given the force and accleration range limits, a Bently Nevada 25-mm-diam noncontracting proximeter was used to measure the displacement. The complete specifications of the sensors are given in Table 2.

The shaker, test article, and sensors were aligned vertically as illustrated in Fig. 5. One end of the test article, a joint in flexure, was rigidily clamped to the test stand. Force was applied to the test article through the force transducer and a thin flexure. The accelerometer was coaligned with the force transducer on the opposite side of the test article. The displacement transducer was coaligned beneath the accelerometer and mounted on a nonrotating micrometer. The steel target for the displacement transducer was mounted on the back of the accelerometer. The test stand supporting the shaker, joint, and proximeter was constructed of steel I-beams affixed to the laboratory wall. Because the measurement of the force was made at the point of application to the test article, deflection along the load path from the shaker to the joint through the test stand are unimportant. These were assured by the large stiffness of the test stand.

The displacement transducer was calibrated using the micrometer movement. The remaining sensors were dynamically calibrated using a proof mass suspended from the force transducer in place of the joint in Fig. 5 with the displacement transducer used as reference. A detailed error analysis of the transmitted force errors as a function of frequency indicated that the transmitted force error was relatively constant (approximately 1.7%) below the first fundamental frequency of the test article. However, the errors were shown to increase rapidly above the fundamental frequency.[5]

Table 4 Pinned joint reference dimensions, mm

$x_p = 55.63$	$x_t = 327.15$
$x_f = 246.89$	$d_0 = 31.75$

Table 5 Identified parameters of the notched rod

Max amp, mm	Freq, Hz	K_1 kN/m	ω_0, Hz
0.8	10	120.4	58.76
2.9	10	119.0	58.42
1.0	10	123.8	59.58
3.0	10	117.9	58.14
0.8	25	120.2	58.71
2.9	25	119.4	58.51
0.7	50	118.3	58.24
0.4	100	121.6	59.05
Average		120.1	58.68
RMS error, %		±1.49	±0.747

Test Articles

In order to demonstrate the effectiveness of the force-state mapping technique in actual experimental conditions, it was used to determine the dynamic characteristics of three test articles fabricated from 2024 aluminum. These articles exhibited properties ranging from those of a simple spring mass system to those more representative of a joint of a deployable structure. The simpest test article was a cylindrical aluminum rod, a small section of which was machined (notched) so that it was also cylindrical but of smaller diameter, producing bending primarily in the notched region. See Fig. 6 and Table 3.

While the notched rod model is a useful test article, it is not representative of space structure joints. Typical joints will have a pin or ball about which the joint will rotate on deployment and, in general, such joints will not have large linear restoring forces. The test article used to model this behavior is shown in Fig. 7 and Table 4. Rounded male and female notches were machined to allow one-degree-of-freedom motion about a pin joining the two sections. This system provided the source of the friction nonlinearity.

In a realistic deployable joint, some additional type of restraining system will be included. An example may be a sleeve that slides in place over the joint to limit rotational motion. Therefore, the final test model included a thin sleeve

Table 6 Identified parameters of the pinned joint

Max amp, mm	Freq, Hz	K_1 kN/m	F_F, N
3.1	10	9.259	7.398
2.1	25	11.834	6.165
Average		10.547	6.782
RMS error, %		±12.2	±9.1

Table 7 Identified parameters of the pinned joint with sleeve

Max amp, mm	Freq, Hz	K_1 kN/m	B_1 N·s/m	K_3 GN/m^3	F_F N
1.7	10	25.11	246.4	16.30	2.470
2.7	10	17.65	180.9	12.60	3.485
2.0	25	35.14	173.6	10.33	—
3.6	25	21.90	138.1	9.52	1.104
Average		24.95	184.8	12.19	2.351
RMS error, %		±25.9	±21.2	±21.6	±41.5

(3.175 mm thick) clamped rigidly at the base of the joint and extending 122.43 mm from the clamp with approximately 0.79 mm in radius clearance. Each of the three test articles was tested with modulated input frequencies of 10, 25, 50 and 100 Hz in order to determine the presence of frequency-dependent transmitted force properties. The tests run with 10 and 25 Hz forcing frequency were also tested at different amplitudes to assess amplitude-dependent effects.

Experimental Results

Notched Rod Specimen

The notched rod test article was a simple spring mass system that should have produced a planar force-state map. Experimentally determined force-state maps of the notched rod results appeared almost identical to Fig. 1 and are therefore not shown. The complete curve fit results of the notched rod tests are, however, shown in Table 5.

The average stiffness value computed from Table 5 is shown to be very precise with a root mean square error of 1.49%, which is below the total system error of 1.73%. The average stiffness is also fairly accurate in that a static stiffness test yielded a stiffness of 110.6 kN/m. Additionally, an analytic static beam analysis indicated a stiffness of 113.3 kN/m. The fact that the force-state stiffness is slightly higher than both other predictions and that the frequency calculated using the identified system mass is slightly lower than the measured value (60.41 Hz from free decay) can both be due to a slight error in the mass estimate.

Pinned Joint Specimen

The first pinned joint model represents a typical deployable joint with no restraining mechanism other than friction between the contacting surfaces within the joint. The transmitted force characteristics of the pinned joint specimen forced at 10 Hz is shown in Fig. 8. Rather than display the commonly expected friction shape of a single force step at zero velocity, the force-state map shows what appears to be a secondary friction step encountered at higher velocities. This could be due to a slight mismatch of the two surfaces of the joint or microslip phenomena. The complete curve fit results of stiffness and Coulomb friction for the pinned joint model are given in Table 6. The computed friction values of Table 6 are average values over the entire test and will not describe the detail of multiple friction zones. However, the force-state mapping technique does provide an accurate representation of a highly nonlinear system.

Pinned Joint with Sleeve Specimen

The final model was the pinned joint with a thin restraining sleeve to restrict rotations. The transmitted force characteristics at 25 Hz for this model are shown in Fig. 9. The force-state map clearly shows a primary friction shift at zero velocity and the secondary friction region can be distinguished in the positive velocity region. The force-state map also clearly illustrates the presence of a cubic hardening spring. A linear viscous damping effect is also noticeable on the force-state maps. The complete curve fit decomposition of the transmitted force of this model is given in Table 7.

While the rms errors in Table 7 are large, the usefulness of the system cannot be judged solely by observing the errors. To better assess the value of the identified parameters, consider the reconstruction of Fig. 9 from those parameters. The original two-dimensional projection of the force-state map onto the force-displacement plane and the reconstructed version are shown in Fig. 10. The first fit is a simple linear and cubic spring function that closely matches the shape, but has no dissipative properties. The second fit then includes friction and produces the expected hysteresis step when the displacement changes direction, i.e., when the velocity changes sign. Finally, with the addition of linear viscous damping, the fourth graph becomes the fully reconstructed signal. Notice that the system transmitted force characteristics have been very accurately reproduced from the measured data. Additionally, what might have originally appeared as a memory effect has been represented well with state-dependent linear viscous damping and Coulomb friction.

Conclusions

The purpose of this paper was to present and verify the force-state mapping technique as a method of identifying nonlinear response in models of joints on space structures. The formulation of the technique has been shown to produce unique, superposable surfaces, called force-state maps, that are characterized only by the system parameters and are not explicitly dependent on the time histories of the state or the frequency of the applied force for the majority of common nonlinearities. For a small class of nonlinearities that exhibit true memory effects, a higher-order force-state map can be created for memory effects linearly related to the state. For memory effects not linearly related, system parameters can be obtained by testing at appropriate frequencies and amplitudes. By using curve fit programs to fit a surface to the force-state map, the system parameters can be retrieved for the entire surface or a small operating region of it. The data necessary to construct the force-state map can be estimated from incomplete measurements using conventional instrumentation and equipment.

To demonstrate the force-state mapping technique, a series of nonlinear response simulations were conducted and the identified system parameters were compared with their actual values. In this set of tests, when the mass and the type of nonlinearity were known explicitly and the measurements were relatively noise free, the force-state mapping technique was shown to identify the primary linear and nonlinear system parameters to within 1%.

Finally, to demonstrate the force-state mapping technique when the measurements may be noisy and the mass and the exact form of the nonlinearities are not well known, three separate experimental models were tested. The models increased in complexity from a lightly damped spring mass system to a pinned joint with friction and cubic stiffness. The identified parameters of the first model were shown to be reproducible and consistent at different frequencies. The final two tests were based on a pinned joint model and were dominated by friction. No analytic model describing the friction in the joint was available for comparison with the identified parameters; however, the force-state maps were very distinct in the description of split friction regions in the state

space, indicating friction that is not a simple Coulomb type. All of the force-state maps accurately depicted the parameters of the system and the measured parameters accurately reproduced the transmitted force characteristics.

Appendix: State Estimation Filter

The application of state estimation techniques requires that the system dynamics be written in state space form with the measurements expressed as observations as

$$\dot{x} = Ax + Bu + v \tag{A1}$$

$$y = Cx + w \tag{A2}$$

where v and w describe the noise in the accelerometer and displacement transducer, respectively. The standard feedback estimation formulation for the state estimates $\hat{x}$ is of the form

$$\dot{\hat{x}} = A\hat{x} + Bu + K(y - C\hat{x}) \tag{A3}$$

where $K = [k_1, k_2]^T$ represents the desired feedback gains of the estimator. The gains K can be chosen to produce a desired steady-state response. Rewritting the equations in terms of the dynamics of the error signal,

$$\dot{\epsilon} = [A - K \cdot C] \cdot \epsilon + v - K \cdot w \tag{A4}$$

where $\epsilon = x - \hat{x}$. The feedback gains k_1 and k_2 can be uniquely determined to produce any desired frequency and damping ratio of the error signal dynamics. However, the second-order system allows for steady-state errors in the state estimates. At steady state, $\dot{\epsilon} = 0$ and

$$\epsilon_{ss} = -[A - K \cdot C]^{-1}\{v - K \cdot w\} \tag{A5}$$

$$\begin{bmatrix} \epsilon_d \\ \epsilon_v \end{bmatrix}_{ss} = \frac{1}{k_2} \begin{bmatrix} 1 \\ k_1 \end{bmatrix} \eta_a - \begin{bmatrix} 1 \\ 0 \end{bmatrix} \eta_d \tag{A6}$$

In the above formulation, a steady-state bias in η_a will always produce a steady-state error in ϵ_d and ϵ_v. To reduce this effect efficiently, an augmented feedback error estimate can be added. This augmented state is equivalent to an integral trim term in the accelerometer feedback. The new augmented state estimation equations then become

$$\begin{bmatrix} \dot{x} \\ \ddot{x} \\ \dot{\eta}_a \end{bmatrix} = \begin{bmatrix} 0 & 1 & 0 \\ 0 & 0 & 1 \\ 0 & 0 & 0 \end{bmatrix} \cdot \begin{bmatrix} x \\ \dot{x} \\ \eta_a \end{bmatrix} + \begin{bmatrix} 0 \\ 1 \\ 0 \end{bmatrix} \ddot{x}_m + \begin{bmatrix} 0 \\ 0 \\ 1 \end{bmatrix} \dot{\eta}_a \tag{A7}$$

$$y = [1 \quad 0 \quad 0] \cdot \begin{bmatrix} x \\ \dot{x} \\ \eta_a \end{bmatrix} + [1]\eta_d \tag{A8}$$

where again Eqs. (A7) and (A8) are strict identities and do not depend on any assumptions concerning the state variables or the structural system being tested. Following the same procedure as with the second-order system, the steady-state error then becomes

$$\epsilon_{ss} = \begin{bmatrix} \epsilon_d \\ \epsilon_v \\ \epsilon_\eta \end{bmatrix} = - \begin{bmatrix} 1 \\ 0 \\ 0 \end{bmatrix} \eta_d + \frac{1}{k_3} \begin{bmatrix} 1 \\ k_1 \\ k_2 \end{bmatrix} \dot{\eta}_a \tag{A9}$$

The accelerometer bias is the dc component of the accelerometer and has therefore been eliminated from the steady-state error in both the displacement and velocity estimates. A constant rate error (drift) is the first-order error that could affect the estimates; however, the time scale associated with drifts is generally much larger than that associated with the test.

The error due to the displacement measurement noise is the same as in the analysis without the augmented state. The displacement noise has no affect on the velocity estimate and affects the displacement estimate as it would without estimation. Therefore, without adversely affecting the displacement measurement, the accelerometer and displacement transducer have been used to improve the velocity estimate by removing any steady-state error due to an accelerometer bias. The selection of k_1, k_2, and k_3 for a given test were made such that the error signal decayed with a frequency three times the highest frequency associated with the test and such that the exponentially decaying component of the error decayed to 5% its original value in 20 time steps.

Acknowledgments

This research was sponsored by NASA Grant NAGW-21 from NASA Headquarters, Washington, DC, with Mr. Samuel Venneri serving as Technical Monitor. The authors would also like to acknowledge the assistance of the staff of the Structural Dynamics Branch at the NASA Langley Research Center, particularly Dr. Garnett Horner, Dr. Jer-Nan Juang, and Richard S. Pappa.

References

[1]Juang, J. and Pappa, R. S., "An Eigensystem Realization Algorithm (ERA) for Modal Parameter Identification and Model Reduction," *Journal of Guidance, Control, and Dynamics*, Vol. 8, Sept.-Oct. 1985, pp. 620-627.

[2]Horta, L. G. and Juang, J., "Identifying Approximate Linear Models for Simple Nonlinear Systems," *Journal of Guidance, Control, and Dynamics*, Vol. 9, July-Aug. 1986, pp. 385-390.

[3]Ewins, D. J. and Sidhu, H., "Modal Testing and the Linearity of Structures," *Mecanique Materiaux Electricite*, No. 389-390-391, May-July 1982, pp. 297-302.

[4]Soni, M. L. and Agrawal, B. N., "Damping Synthesis for Flexible Space Structures Using Combined Experimental and Analytical Models," AIAA Paper 85-0779, April 1985.

[5]O'Donnell, K. J. and Crawley, E. F., "Identification of Nonlinear Parameters in Space Structure Joints Using the Force-State Mapping Technique," Space Systems Laboratory, Massachusetts Institute of Technology, Cambridge, Rept. 16-85, July 1985.

[6]Crawley, E. F. and Aubert, A. C., "Identification of Nonlinear Structural Elements by Force-State Mapping," *AIAA Journal*, Vol. 24, Jan. 1986, pp. 155-162.

[7]Hertz, T. J. and Crawley, E. F., "Displacement Dependent Friction in Space Structure Joints," *AIAA Journal*, Vol. 24, Dec. 1985, pp. 1998-2000.

[8]McKillip, R. M. Jr., "Periodic Control of the Individual-Blade-Control Helicopter Rotor," *Vertica*, Vol. 9, No. 2, 1985, pp. 199-225.

[9]Kwakernaak, H. and Sivan, R., *Linear Optimal Control Systems*, Wiley, New York, 1972, pp. 328-373.